Glypiation enables FGF to self-regulate its tissue-specific dispersion and interpretation through cytonemes

Lijuan Du, Alex Sohr, Sougata Roy*

Department of Cell Biology and Molecular Genetics; University of Maryland, College Park, MD 20742

*Corresponding author: sougata@umd.edu

Keywords: FGF, bidirectional signaling, GPI anchor, cytonemes, synapse, self-organization, Bnl, cell-adhesion-molecule (CAM), *Drosophila*

Short Title: Bidirectional FGF-FGFR signaling at cytoneme contacts

ABSTRACT

During development, a handful of signals sculpt diverse tissue architectures. How the same signal produces different tissue/context-specific information and outcomes is poorly understood. We explored the basis that programs tissue-specific FGF dispersion and interpretation by cytoneme-mediated contact-dependent communication. Although a *Drosophila* FGF was thought to be freely secreted, we discovered that it is glypiated and GPI-anchored on the source cell surface, which inhibits non-specific secretion but facilitates tissue-specific cytoneme contact formation and contact-dependent release. For long-distance signaling, source and recipient cells extend FGF-containing and FGFR-containing cytonemes that contact and recognize each other by CAM-like receptor-ligand binding. FGF-FGFR binding reciprocally induces forward and reverse signaling in recipient and source cells, responses of which polarize their cytonemes toward each other to mutually self-sustain contacts. FGFR-bound FGF's subsequent unanchoring hand-delivers FGF to receiving cytonemes and dissociates contacts. Thus, while cytonemes spatiotemporally control FGF dispersion/interpretation, FGF self-regulates its tissue-specific signaling by controlling cytonemes.

Introduction

During morphogenesis, cells spatiotemporally coordinate their differentiation, function, and patterns of organization by communicating with signaling proteins or morphogens (*1*). Genetic and molecular characterization of pattern-forming genes revealed that there are only a handful of morphogenetic signals, including Fibroblast Growth Factor (FGF), Hedgehog (Hh), Wingless (Wg)/Wnt, Epidermal Growth Factor (EGF), and Decapentaplegic (Dpp - a BMP homolog). These signals disperse across tissues to form concertation gradients and, upon binding to receptors in recipient cells, activate gene regulatory pathways in a dose-dependent manner to control coordinated responses in cells (*1*). Strikingly, activity of this same set of signals and pathways is sufficient to specify a plethora of cell types and tissue patterns in diverse contexts, suggesting their adaptive, context-specific functions. This raises a question on the exact nature of the morphogenetic cues, especially in the way they inform cells of their spatiotemporal identity, activity, and dynamic organization. Despite myriads of examples of context-specificity, the mechanisms by which a signal might program and induce diverse tissue-specific information and outcomes remained an open question.

The ability for a tissue to interpret a specific signal or 'competence' is an actively acquired state in responding cells (*2*). In contrast, the signals are traditionally envisioned to be non-selectively secreted in the extracellular space and randomly dispersed by passive diffusion. However, recent advances in live microscopy revealed that during development, cells actively regulate target-specific signal dispersion by dynamically extending actin-based signaling filopodia named cytonemes (*3*). Cytonemes and cytoneme-like signaling filopodia were discovered in different vertebrate and invertebrate morphogenetic, stem cell, and disease contexts (*4-9*). Prevalence of signaling filopodia and their essential roles for most signals, including Hh, Dpp, FGF, EGF, and Wnt suggest that the contact-based signaling is an evolutionarily conserved, basic mechanism.

Despite being contact-dependent, cytoneme-mediated signaling can produce diverse tissue-specific signal dispersion and signaling patterns (*10*, *11*). For instance, a

Drosophila FGF, Branchless (Bnl) is expressed by a group of cells in the larval wing imaginal disc, but it forms a long-range dispersion gradient only within the disc-associated air-sac primordium (ASP) that expresses the Bnl receptor Breathless (FGFR/Btl) (*10*, *12*). The ASP extends Btl-containing cytonemes that directly contact Bnl-expressing disc cells and take up Bnl (*10*). Recipient-specific shapes of Bnl gradients emerge due to signaling through a graded number of Bnl-receiving cytonemes along the distal-proximal axis of the ASP. On the other hand, varied Bnl signaling levels in different ASP regions activate different target genes that differentially feedback control formation of Bnl-receiving cytonemes, establishing the graded pattern of Bnl-receiving cytonemes. Consequently, robust recipient-specific shapes of signal and signaling patterns emerge in precise coordination with ASP growth and patterning.

Initiation of cytoneme-mediated patterning and its tissue-specificity depend on where and when cytonemes establish signaling contacts (*10*). However, little is known about how tissue-specific signaling contacts are established and controlled in space and time and why and how secreted signals are release only via cytoneme contacts. In this paper, we addressed these questions using Bnl/FGF signaling in the *Drosophila* ASP. Bnl has a single receptor, Btl, and its activation induces MAPK signaling. Despite apparent similar stimulation, genetic analyses have revealed multiple functions for Bnl, such as acting as a mitogen, morphogen, or chemoattractant in diverse contexts, including stem cells, trachea, neuron/glial, blood cells, and cancer (*8*, *10*, *12-18*). We discovered that while cytonemes control tissue-specific Bnl distribution and signaling, Bnl glypiation programs the spatiotemporal origin, distribution, and plasticity of cytoneme contacts, thereby self-regulating its tissue-specific dispersion and functions. This provides a new mechanistic insight into how the context-specific signaling is programmed and realized by self-organizing the signal dispersion process.

Results

Bidirectional contact matchmaking of Bnl-sending and Bnl-receiving cytonemes.

Inter-organ Bnl signaling between the ASP and wing disc provides a simple genetic system for an unbiased interpretation of tissue-specific dispersion as Bnl is produced in

the wing disc and travels across a layer of interspersed myoblasts to the overlaying ASP, which expresses its only receptor, Btl (Fig. 1A,B) (*10*). Bnl is a secreted FGF family protein, but externalized Bnl (Bnl^{ex}) detected by anti-Bnl immunostaining of non-permeabilized imaginal disc preparations (αBnl^{ex}; Materials and Methods) is not broadly distributed in the myoblasts and extracellular plane of its wing disc source. Instead, Bnl^{ex} puncta were exclusively localized tissue-specifically only on the basal surface of wing disc source cells, and recipient ASP and ASP cytonemes (Figs. 1A,C). These images are consistent with tissue-specific transport of Bnl^{ex} to the ASP in a receptor-bound form along the surface of ASP cytonemes (*10*). More strikingly, compared to the relatively large *bnl* expression domain, Bnl^{ex} puncta on source cells were asymmetrically congregated at the sites where Btl-containing ASP cytonemes established contacts.

To examine if the distribution of Bnl in source cells is uniform or spatially biased toward the ASP, we examined wing discs that overexpress Bnl:GFP and mCherryCAAX driven by *bnl-Gal4*. Although both constructs were expressed under the same driver, only Bnl:GFP puncta were highly enriched in the ASP-proximal source area (Figs. 1D-D"; S1A,A'). Furthermore, wing discs that expressed Bnl:GFP either under endogenous control (*bnl:gfp*^{endo} allele; (*10*)) or under *bnl-Gal4*, revealed that source cells in the ASP-proximal area extend Bnl:GFP-containing filopodia or cytonemes toward the ASP (Figs. 1D; S1B). These results suggest that the cellular components in source cells responsible for Bnl secretion, display, and/or delivery are polarized toward the ASP.

Because Bnl-containing filopodia from source cells had not been reported before, we first examined their functions. Source cytonemes were detected in unfixed wing discs that expressed a fluorescent membrane marker (e.g., CD8:GFP or CherryCAAX) either in all of the *bnl*-expressing cells or in small clones of cells within the Bnl expressing area. Three-dimensional XZY image projections revealed that each of the Bnl-expressing columnar cells proximal to the ASP extended ~2-4 short (<15 μm) cytonemes perpendicularly from their basal surface (Figs. 1F-H; S1C-E; Movie S1; Table S1). The organization of the source cells therefore can be described as polarized for basal Bnl presentation with basal projections extending toward the ASP. This

organization is mirrored in the ASP, which, as we previously reported, exhibits polarized Btl synthesis, Bnl reception, and cytoneme orientation toward source cells (*10*). Thus, signal-sending and -receiving components polarize to face each other, forming a tissue-level niche at the ASP:source interface to promote cytoneme-mediated interactions.

Time-lapse imaging of ex vivo cultured wing discs revealed that the ASP and source cytonemes orient toward each other and transiently contact each other's tips, bases, or shafts as they dynamically extend and retract (Figs. 1I-M; S1H-O; Table S2; Movies S2a,b). Both cytoneme types had dynamic and repeated cycles of contact association-dissociation, but source cytonemes had a shorter lifetime than ASP cytonemes. Importantly, such transient cytoneme:cytoneme contacts at the interface of ASP and source cells are persistent throughout larval development (Fig. S1H-M). This is consistent with the model of a cytoneme signaling niche at the interface of the ASP abd wing disc source.

Based on our previous results on cytoneme-mediated Bnl uptake in the ASP (*10*), Bnl is likely to be exchanged at the inter-cytoneme contact sites. However, it was technically challenging to capture Bnl exchange via dynamic cytoneme interactions. Therefore, we genetically ablated the source cytonemes and analyzed non-autonomous Bnl dispersion into the ASP. Similar to ASP cytonemes (*19*), the formation of source cytonemes could be induced by overexpressing an actin modulator formin, Diaphanous (Dia), and were suppressed by *dia* knockdown in the source (Fig. 2A-E). Notably, a constitutively active form of Dia, DiaΔDAD-GFP, selectively localized at the ASP-proximal source area and at cytoneme tips, which is consistent with a localized increase in f-actin polymerization activity in the cytoneme-producing source area (Figs. 2C; S1F,G). Ablating source cytonemes in *bnl:gfp*^{endo} larvae by *dia RNAi* expression in the source led to the non-autonomous reduction of Bnl:GFP^{endo} uptake in the ASP, leading to abnormally stunted ASPs (Fig. 2F-H). This suggested that source cytonemes are important to selectively deliver Bnl to ASP cytonemes and cells.

Inter-cytoneme Bnl exchange is consistent with previous reports that Hh and Wg are both sent and received by cytonemes (*20-22*). However, dynamic interactions of Bnl-exchanging cytonemes that are convergently polarized toward each other might also indicate a possibility of contact-dependent reciprocal guidance of source and recipient cytonemes. To test this possibility, we first ablated source cytonemes by *dia RNAi* expression and analyzed the effects on ASP cytonemes. The absence of source cytonemes non-autonomously reduced the long, polarized ASP tip cytonemes that make signaling contacts with the source (Fig. 2I-K). Since randomly oriented short ASP cytonemes were unaffected, Bnl-sending cytonemes are required for the formation of only polarized Bnl-receiving cytonemes from the ASP.

To determine if ASP cytonemes also influence the polarity of source cytonemes, we removed ASP cytonemes by expressing a dominant-negative form of Btl (Btl:DN) in the trachea, as reported previously (*12*). A complete loss of the ASP and ASP cytonemes also led to a corresponding non-autonomous loss of polarized source cytonemes (Fig. 2L). Btl:DN expression occasionally produced partial dominant-negative effects, yielding stunted ASPs with few polarized cytonemes. Strikingly, the appearance of polarized cytonemes in each of these ASPs correlated with the appearance of equivalent numbers of source cytonemes, making stable cytoneme:cytoneme contacts (Fig. 2M-O). These results suggested that the inter-cytoneme contacts induce ASP cells to extend Btl-containing cytonemes toward the source and induce source cells to extend Bnl-containing cytonemes toward the ASP. Thus, ASP and source cytonemes reciprocally guide each other to establish contacts and/or selectively stabilize these contacts.

Glypiation tethers Bnl to the source cell surface.

Note that Btl:DN cannot signal due to the lack of its intracellular domain, but can bind to Bnl with its extracellular portion (*12*). When we probed for the distribution of externalized Bnl in the Btl:DN expressing samples, Bnl^{ex} were selectively enriched on the source and recipient cytonemes that established stable contacts with each other (Fig. 2P-P"). The enrichment of surface Bnl^{ex} at the inter-cytoneme contacts suggested an interesting

possibility that the Btl-Bnl binding that is required for intercellular Bnl exchange might also be the molecular basis for the source and recipient cytoneme contact formation. However, this model assumes that Bnl is retained on the source cell surface to act as a cell recognition molecule. How might a secreted protein be retained exclusively on the source cell surface, without being randomly dispersed in the extracellular space?

A possible mechanism emerged from studies of the surface distribution of various chimeric Bnl:GFP constructs expressed in cultured *Drosophila* S2 cells. Bnl is synthesized as a 770 amino acid protein and is cleaved in the Golgi by Furin1 at residue 164 prior to the externalization of its truncated C-terminal signaling portion (Fig.3A; (*23*)). Therefore, when S2 cells expressed a chimeric Bnl:HA_1GFP_3 construct with HA (site 1) and GFP (site 3) flanking the Furin cleavage site, the HA-tag localized to the Golgi and the truncated Bnl:GFP_3 fragment was externalized. These observations led us to hypothesize that a Bnl:$GFP_3Cherry_c$ construct (Fig. 3A), which has an in-frame C-terminal mCherry fusion, would externalize the truncated C-terminal fragment marked with both GFP and mCherry. Unexpectedly, most membrane-localized Bnl:GFP_3 puncta (detected with αGFP^{ex}) lacked mCherry, indicating the possibility of a second intracellular cleavage at the C-terminus of the Bnl protein prior to externalization (Fig. 3B-B'").

Bioinformatic analyses (see Methods) revealed that the Bnl C-terminal tail has a 20 amino acid hydrophobic segment immediately adjacent to a hydrophilic region (Fig. 3A,A'), similar to signal sequences of pro-GPI-anchored proteins (pro-GPI-APs). The signal sequences of pro-GPI-APs are cleaved and replaced with a GPI moiety in the endoplasmic reticulum (ER) prior to trafficking to the cell surface, where these proteins are anchored to the outer leaflet of the plasma membrane (*24*). Because the presence of C-terminal tags does not prevent glypiation of pro-GPI-APs (*25*), we surmised that Bnl glypiation might explain C-terminal cleavage in Bnl:$HA_1GFP_3Cherry_c$ and surface distribution of only Bnl:GFP_3. To investigate Bnl glypiation, we followed a standard phosphoinositide phospholipase C (PI-PLC) assay (Figs. 3C-E; S2B-I; see Methods). PI-PLC specifically cleaves most GPI moieties between the phosphate and glycerol

backbone, leading to the shedding of GPI-APs from the cell surface. When S2 cells expressed Bnl:GFP_3, Bn:HA_1GFP_3 (henceforth Bnl:GFP), untagged Bnl (detected with αBnl^{ex}), and a control GFP-GPI construct (*26*), all constructs localized on the cell surface and were shed by PI-PLC treatment (Figs. 3C,C',E; S2B,F,I). In contrast, PI-PLC did not shed a constitutively active *Drosophila* EGF construct, cSpitz:GFP (Fig. 3C,C',E), which is tethered to the cell membrane due to palmitoylation (*27*).

In silico analyses (see Methods) identified S^{741} of Bnl as a probable glypiation site (ω-site). In S2 cells, Bnl:GFP mutant constructs that either lacked the C-terminal 40 amino acid residues (Bnl:GFPΔC), or contained mutated ω, $\omega{+}1$, and $\omega{+}2$ sites (Bnl:GFP-ω^m) failed to localize on the producing cell surface, even in the absence of PI-PLC treatment (Figs. 3C-E'; S2G,I). However, when we added the transmembrane domain of the mammalian CD8a protein to the C-terminus of Bnl:GFPΔC, the protein (henceforth Bnl:GFPΔC-TM) was tethered to the cell surface irrespective of PI-PLC treatment (Figs. 3C-E; S2H,I). To test the functionality of the Bnl C-terminal signal sequence, we fused it to the C-terminus of a secreted sfGFP that also has the Bnl N-terminal signal peptide (*10*). The resultant construct, bGFP-GPI, had the same localization as a GPI-AP and was sensitive to PI-PLC treatment (Fig. 3C-E). Together, these results confirmed that Bnl is a GPI-AP and that it has a C-terminal signal sequence that is replaced by a GPI moiety after cleavage at S^{741}.

To determine if Bnl is also glypiated in native wing disc cells, we performed surface αBnl^{ex} immunostaining on ex vivo cultured wing discs (*10*) before and after PI-PLC treatment (Fig. 3F-R). Native Bnl^{ex} puncta were concentrated on the disc source cells near ASP cytonemes, but their levels were significantly reduced after PI-PLC treatment (Fig. 3F-H). When Bnl and the Bnl:GFP, Bnl:GFPΔC, and Bnl:GFPΔC-TM constructs were overexpressed under *bnl-Gal4*, PI-PLC treatment significantly reduced levels of Bnl^{ex} and Bnl:GFP^{ex}, but not Bnl:GFPΔC-TM^{ex} (Fig. 3I-R). Similar to the observations in S2 cells, Bnl:GFPΔC^{ex}, was not concentrated on the surface of source cells even without PI-PLC treatment (Figs. 3N-O',R). Instead, randomly dispersed Bnl:GFPΔC^{ex} puncta surrounding the disc source suggested that Bnl:GFPΔC^{ex} is

readily secreted into extracellular space. These results confirmed that Bnl is GPI-anchored to the wing disc source cells.

Bnl's GPI anchor ensures tissue-specific Bnl dispersion and signaling.

To investigate if GPI anchoring on the source surface specifies Bnl's tissue-specific distribution, we imaged GPI-modified (Bnl:GFP) and non-GPI-modified (Bnl:GFPΔC and Bnl:GFPΔC-TM) constructs expressed from the mCherrryCAAX-marked wing disc Bnl source. Overexpressed Bnl:GFP was localized almost exclusively in disc producing cells and target-specifically dispersed into the ASP (Fig. 4A; Movie S3). In contrast, Bnl:GFP mutants that lack a GPI anchor (Bnl:GFPΔC and Bnl:GFPΔC$_{168}$) were also dispersed around disc source cells, without apparent spatial specificity (Fig. 4C; Movie S4). On the other hand, Bnl:GFPΔC-TM puncta were restricted to only source cells and a few ASP cells that were directly juxtaposed to the source (Fig. 4B; Movie S5). Unlike Bnl:GFP in ASP cells, these Bnl:GFPΔC-TM puncta in the ASP were abnormally colocalized with the source cell membrane, indicating a defect in release from their TM tether (Figs. 4B; S3A-B'). These results suggest that Bnl's GPI anchoring inhibits only random non-specific release but facilitates its tissue-specific dispersion.

To investigate if tissue-specific Bnl dispersion is critical for signaling outcomes, we imaged the correlation of the spatial distribution patterns of GPI-modified and non-GPI-modified Bnl:GFP variants and that of the MAPK signaling. When Bnl:GFP was overexpressed from the wing disc source under *bnl-Gal4*, all of the ASP cells received Bnl:GFP and induced MAPK (nuclear dpERK localization) signaling (Figs. 4D,K; S3C-E'). As expected, Bnl:GFPΔC-TM distribution and activity was restricted to only a small number of ASP tip cells (Figs. 4E,K; S3C). In contrast, a significant number of cells that received Bnl:GFPΔC in the ASP failed to activate nuclear MAPK signaling (Figs. 4F,K; S3F,G). It is clear that the precise coordination of signal dispersion, signaling, and growth was lost with Bnl:GFPΔC expression. Interestingly, similar to Bnl:GFP, Bnl:GFPΔC could also induce ASP overgrowth and it is likely that the growth is controlled by unknown interactions of multiple signaling pathways.

To analyze these signaling anomalies further, we generated ectopic gain-of-function (GOF) clones of Bnl:GFP, Bnl:GFPΔC-TM, or Bnl:GFPΔC directly within the ASP epithelium. We scored only small sized clones (2-3 cell diameter) within the ASP stalk or transverse connective (TC) that normally do not receive Bnl or activate MAPK signaling. Ectopic Bnl:GFP GOF clones in the ASP stalk induced dpERK within a uniform distance of 2-3 cells surrounding the clone (Figs. 4H,H',K; S3K). In contrast, Bnl:GFPΔC-TM moved from its clonal source to only a few of the juxtaposed cells to induce MAPK signaling in them and to organize them into an ectopic tracheal outgrowth (Figs. 4I,K; S3H,I,K). On the other hand, Bnl:GFPΔC GOF clones had wider signal dispersion than Bnl:GFP, but only a few random signal-receiving cells had dpERK (Figs. 4J,K; S3J,K). Collectively, all these results show that the precise spatial correlation of signal dispersion, interpretation, and growth require GPI anchored retention of Bnl on the source surface. These results also show that the GPI anchor enables Bnl to generate adaptive, context-specific spatial patterns depending on the location of the source and recipient cells.

To further test if the presence or absence of a surface tether is critical to determine context-specific outcomes, we took advantage of Bnl's ability to attract tracheal branch invasion on its source cell surfaces (*14*). According to the chemo-gradient model that has been proposed for Bnl's function as an inducer of tracheal branch migration, random extracellular Bnl:GFPΔC dispersion might promote tracheal chemotaxis toward its source. To examine, we ectopically expressed the GPI-modified and non-GPI-modified Bnl:GFP variants in the larval salivary gland, a non-essential, trachea-free organ that normally does not express Bnl (Fig. 4L-O; see Methods) (*23*). Surprisingly, although Bnl:GFP and Bnl:GFPΔC-TM induced tracheal invasion and branching into the signal-expressing salivary glands, Bnl:GFPΔC did not. Bnl:GFPΔC-TM is a TM-tethered Bnl:GFPΔC, yet it induced extensive tracheation on salivary glands. Thus, tracheal migration and branching phenotypes do not correlate with the random extracellular presence of extracellular Bnl. On the contrary, increased tracheal invasion and branching on producing cells do correlate with the levels of Bnl available on the basal surface of source cells. As shown in Figure 4P-S, the amount of Bnl:GFPΔC on the

surface of the salivary gland is significantly less than either Bnl:GFP or Bnl:GFPΔC-TM. These results show that retention of Bnl on the source surface is the key factor for Bnl target-specific dispersion and interpretation. We proposed that cytoneme-mediated exchange between source and target cells is the mechanism that links source surface Bnl retention with its long-range context-specific dispersion and interpretation and that GPI-anchored Bnl is the driver of the contact-dependent signaling through cytonemes.

GPI-anchored Bnl acts as a CAM to drive bidirectional matchmaking of source and ASP cytonemes.

How does the addition of a GPI moiety enable Bnl to drive dynamic assembly-disassembly of cytoneme contacts and mediate contact-dependent signal release? We tested an idea that GPI-anchored Bnl acts as a cell surface CAM that mediates heterotypic receptor-ligand-dependent target recognition and bidirectional contact matchmaking of cytonemes. This model also predicts that, like other CAMs (*28*), contact-dependent Btl-Bnl signaling is bidirectional, which would reciprocally activate source and recipient cells to project cytonemes toward each other to form signaling contacts. Finally, binding by Btl present on recipient cytonemes also would release Bnl from its anchor to the source membrane and dissociate cytoneme contacts, thereby restricting Bnl release only to the target-specific cytoneme contacts.

Results from Btl:DN experiments corroborated with Btl's role as a CAM (Fig. 2L-P''). Although Btl:DN cannot activate MAPK signaling, it retains the extracellular Bnl-binding domain (*12*), and therefore Btl:DN-containing ASP cytonemes were capable of establishing inter-cytoneme contacts and inducing polarized source cytoneme formation (Fig. 2N-P''). To test if surface-tethered Bnl has CAM-like bidirectional activity, we investigated how GPI-modified and non-GPI-modified Bnl:GFP variants affect source and ASP cytonemes (Figs. 5A-I; S4A-I). Although Bnl:GFP overexpression abnormally brought a large number of source and recipient cells into close proximity due to the ASP overgrowth, both tissues extended polarized cytonemes toward each other (Figs. 5A-C; S4H,I). Increased extension-retraction dynamics of ASP cytonemes suggested high signaling activity (Movie S6; Table S2). In contrast, overexpression of Bnl:GFPΔC

lacked CAM activity and significantly suppressed the formation of long polarized cytonemes in both the source and ASP cells (Figs. 5D-F; S4A,B,H,I). Short cytonemes, when detectable, lacked any directional bias and rarely contained Bnl:GFPΔC. These results are consistent with the idea that GPI-anchored Bnl induces CAM-like bidirectional contact matchmaking.

Importantly, unlike freely dispersed Bnl:GFPΔC, Bnl:GFPΔC-TM induced both ASP and source cells to extend large numbers of long cytonemes that were stably connected with each other via their tips and lateral sides (Figs. 5G-J'; S4C-K; Movies S8-10). The polarized responses induced by Bnl:GFPΔC-TM were stronger than either Bnl:GFP or WT (native Bnl). Bnl:GFPΔC-TM puncta localized at multiple lateral contact interfaces of the source and recipient cytonemes, indicating the increased number and stability of contact sites (Figs. 5G,J-J'; S4E-F; Movies S9-10). The increase in the stability of the contacts might also account for an increase in the intensity of their bidirectional responses. These results show that Bnl surface anchoring, irrespective of the nature of the anchor, is sufficient for its CAM-like bidirectional signaling and contact matchmaking.

To examine whether heterotypic CAM-like Bnl-Btl interactions establish inter-cytoneme contacts, we took advantage of the relatively stable cytonemes produced by Bnl:GFPΔC-TM. Bnl:GFPΔC-TM was expressed in CD4:IFP$_2$-marked wing disc source cells of larvae that also harbored a *btl:cherry^{endo}* knock-in allele (*10*) expressing endogenous Btl:Cherry^{endo} from the ASP. BtlCherry^{endo} puncta localized in close proximity to Bnl:GFPΔC-TM puncta at multiple sites along the length of the juxtaposed source and recipient cytonemes (Fig. 6A-B). These colocalized puncta mimicked the co-clustered organization of receptors and ligands at the inter-cytoneme junctions (Fig. 2P-P''). These results, together with the previous evidence (Fig. 1A-C), show that the CAM-like Btl-Bnl-binding through cytoneme contacts is the basis of contact recognition and bidirectional matchmaking.

GPI anchor ensures Bnl's contact-dependent release and contact plasticity.

Although Bnl:GFPΔC-TM acts as a CAM to induce strong bidirectional responses that manifest in target-specific cytoneme polarity and inter-cytoneme contacts, Bnl:GFPΔC-TM-exchanging cytonemes had a significantly longer lifetime than WT or Bnl:GFP-exchanging cytonemes (Figs. 6C,D; S4J,K; Movies S8-S11; Table S2). Time-lapse live imaging of source and ASP cells showed that the Bnl:GFPΔC-TM-exchanging cytonemes made stable connections that resist signal release, and therefore also resist contact dissociation, leading to cytoneme breakage (Movie S10). Thus, the GPI anchor is required for the release of Btl-bound Bnl at the contact sites. This process is also likely to trigger cytoneme contact dissociation.

This selective release mechanism suggests that the CAM-like function of GPI-anchored Bnl is a prerequisite for Bnl release and subsequent morphogen-like interpretation. As a result, Bnl:GFPΔC-TM exhibits efficient CAM-like cytoneme contact assembly, but is restricted in functional range due to its lack of release at the contact sites (Figs. 4D-K; 6E). Similarly, this explains why Bnl:GFPΔC that lacks CAM activity also fails to induce subsequent morphogen-like patterning of Bnl signaling (Fig. 4D-K). Only the GPI modification integrates both tissue-specific contact formation and contact-dependent release, leading to the diverse context-specific signaling patterns.

DISCUSSION

This study uncovered an elegant programming of a tissue-specific signaling mechanism that is encoded by the lipid-modification of an FGF family morphogen, Bnl and orchestrated by cytoneme-mediated contact-dependent communications. On one hand, it explains how cytonemes can select a specific target to establish signaling contacts, exchange signals at these contact sites, and inform cells where they are, what they should do, and when (Fig. 6E). On the other hand, it shows how glypiation enables the signal to program and drive these cytoneme-mediated events to self-regulate its diverse tissue-specific journey and signaling. We provided evidence that the self-regulatory interplay between signals and signaling cells, controlling each other's location and activity through cytonemes, is essential for context-specific self-organization of signal dispersion and interpretation in coordination with tissue growth.

Traditionally, most secreted signals are envisioned to orchestrate morphogenesis by diffusing away from the source and then activating the receptor and gene-regulatory pathway only in recipient cells. According to this one-way directive from a signal to signaling outcomes, signal retention in the source is inhibitory for its subsequent long-range signal spread and interpretations. In contrast, we discovered that Bnl is GPI anchored to the source cell surface and although this modification inhibits its non-specific release and random diffusion, it facilitates Bnl's target-specific cytoneme-mediated long-range spread and bidirectional signaling.

Mechanistically, GPI-anchored Bnl modulates three interdependent events: cytoneme-mediated target selection, target-specific signal release, and feedback regulations of these processes. We showed that GPI-anchored Bnl on the source cell surface and Btl on the receiving cell surface act as CAMs. This enables Bnl-producing and receiving cells to adhere with and recognize each other by Btl-Bnl binding. However, these cells are situated in two different tissues and are separated in space. Therefore, both Bnl source and recipient cells dynamically extend cytonemes to present Bnl and Btl on their surfaces and recognize each other through Btl-Bnl interactions at their contact sites. The CAM-like Btl-Bnl binding induces forward signaling in the ASP and retrograde signaling in the source, feedback responses of which promote these cells to extend more Bnl-receiving and Bnl-sending cytonemes toward each other and selectively stabilize their mutual contact sites. Our results suggest that by employing these reciprocal cytoneme-promoting feedbacks, source and ASP cells inform each other of their relative locations, polarity, and signaling activities and establish a convergently polarized signaling niche to self-sustain contact-mediated interactions. Here, the molecular, cellular, and tissue level events are interdependent and are integrated by cytoneme contacts.

The process of cytoneme contact assembly is reminiscent of CAM-mediated bidirectional matchmaking of pre-synaptic and post-synaptic filopodial matchmaking that organizes *Drosophila* neuromuscular junctions (*29*). Bidirectional transmission of

information is the basis for neuronal synaptic assembly, plasticity, and functions. However, the purpose of Btl-Bnl-dependent contact recognition is to subsequently release the Btl-bound Bnl at the cytoneme contact sites. Bnl release not only initiates target-specific Bnl delivery and long-range morphogen-like functions in the ASP (*10*) but also initiates cytoneme contact disassembly. Based on functional attributes of GPI-modified and non-GPI-modified Bnl variants, we predict that the plasticity of signaling contacts modulate the levels and duration of Bnl signaling and is also the key for spatiotemporal adaptability/plasticity in the emerging shapes.

Importantly, the GPI anchor enables Bnl to simultaneously modulate both the development of target-specific cytoneme contacts and contact-dependent signal release, thereby mechanistically linking these two events to be interdependent in time and space via signaling contacts. A consequence is that the cause and effects of Bnl signaling can control each other via cytonemes. The same cytoneme contacts that Btl-Bnl binding helps to establish also bring Btl and Bnl molecules together to interact. Thus, not only is the signal exchange cytoneme or contact-dependent, but the cytoneme contacts are also formed signal- or tissue-specifically. Similarly, Bnl and Btl each can act as both a ligand and a receptor for the other and relay information from inside-out and outside-in across the cell membrane. Consequently, contact-dependent Btl-Bnl signaling is bidirectional, specifying functions in both source and recipient cells.

How the local contact-dependent Bnl exchange might self-organize large-scale tissue-specific dispersion/signaling patterns can be explained from our previous findings (*10*). Collectively, these results suggest that cytoneme-mediated signal exchange is designed to induce context-specific self-organization of signaling patterns. Self-organization is an inherent property of living systems. How diffusion and interactions of morphogens might generate self-organized patterns were first theorized by Alan Turing in 1952 (*30*). However, the evidence for a mechanism by which signal dispersion might program self-organizing outcomes remained elusive. This study provides an evidence for a mechanism that is orchestrated by cytoneme-mediated interactions and is encoded by a lipid-modified morphogen.

Post-translational modifications are common to most secreted morphogens. Hh, Wnt, and EGF/Spi are known to be lipid-modified and, therefore, are restricted for secretion and spread (*27*, *31*, *32*). Signals that are not known to be lipidated, including BMPs and many FGFs, need to interact with GPI-anchored glypicans to produce morphogenetic outcomes (*33*, *34*). Proteoglycans restrict free release of the interacting signals and show biphasic activation and inhibition effects on signal spread (*35*). Similar to Bnl, non-lipidated Hh, Spi, and Wnt have unrestricted spread but poor tissue organizing potency, but their TM-tethered forms can induce morphogen-like patterning despite a restricted functional range (*27*, *36-40*). These results suggest a significant role of signal retention in morphogenesis. However, the functional links of the diverse signal retention strategies to either cytoneme-mediated tissue-specific dispersal or context-specific self-organization of signaling need to be examined in the future.

References

1. N. Perrimon, C. Pitsouli, B.-Z. Shilo, Signaling mechanisms controlling cell fate and embryonic patterning. *Cold Spring Harbor Perspectives in Biology*. 4, a005975–a005975 (2012).

2. A. Sagner, J. Briscoe, Morphogen interpretation: concentration, time, competence, and signaling dynamics. *Wiley Interdiscip Rev Dev Biol*. 6, e271 (2017).

3. F. A. Ramírez-Weber, T. B. Kornberg, Cytonemes: cellular processes that project to the principal signaling center in Drosophila imaginal discs. *Cell*. 97, 599–607 (1999).

4. T. A. Sanders, E. Llagostera, M. Barna, Specialized filopodia direct long-range transport of SHH during vertebrate tissue patterning. *Nature*. 497, 628–632 (2013).

5. T. B. Kornberg, S. Roy, Cytonemes as specialized signaling filopodia. *Development*. 141, 729–736 (2014).

6. D. S. Eom, D. M. Parichy, A macrophage relay for long-distance signaling during postembryonic tissue remodeling. *Science*. 355, 1317–1320 (2017).

7. Y. M. Yamashita, M. Inaba, M. Buszczak, Specialized Intercellular Communications via Cytonemes and Nanotubes. *Annu. Rev. Cell Dev. Biol.* 34, 59–84 (2018).

8. S. Fereres, R. Hatori, M. Hatori, T. B. Kornberg, Cytoneme-mediated signaling essential for tumorigenesis. *PLoS Genet*. 15, e1008415 (2019).

9. C. Zhang, S. Scholpp, Cytonemes in development. *Current Opinion in Genetics & Development*. 57, 25–30 (2019).

10. L. Du, A. Sohr, G. Yan, S. Roy, Feedback regulation of cytoneme-mediated transport shapes a tissue-specific FGF morphogen gradient (2018), doi:10.7554/eLife.38137.

11. R. Hatori, T. B. Kornberg, Hedgehog produced by the Drosophila wing imaginal disc induces distinct responses in three target tissues. *Development*. 147, dev195974 (2020).

12. M. Sato, T. B. Kornberg, FGF is an essential mitogen and chemoattractant for the air sacs of the drosophila tracheal system. *Developmental Cell*. 3, 195–207 (2002).

13. D. Sutherland, C. Samakovlis, M. A. Krasnow, branchless encodes a Drosophila FGF homolog that controls tracheal cell migration and the pattern of branching. *Cell*. 87, 1091–1101 (1996).

14. A. Ochoa-Espinosa, M. Affolter, Branching morphogenesis: from cells to organs and back. *Cold Spring Harbor Perspectives in Biology*. 4, a008243–a008243 (2012).

15. F. Chen, M. A. Krasnow, Progenitor outgrowth from the niche in Drosophila trachea is guided by FGF from decaying branches. *Science*. 343, 186–189 (2014).

16. L. Du *et al.*, Unique patterns of organization and migration of FGF-expressing cells during Drosophila morphogenesis. *Dev. Biol.* 427, 35–48 (2017).

17. J. V. Dos Santos, R. Y. Yu, A. Terceros, B. E. Chen, FGF receptors are required for proper axonal branch targeting in Drosophila. *Mol Brain*. 12, 84 (2019).

18. M. Destalminil-Letourneau, I. Morin-Poulard, Y. Tian, N. Vanzo, M. Crozatier, The vascular niche controls Drosophila hematopoiesis via fibroblast growth factor signaling. *Elife*. 10, 45 (2021).

19. S. Roy, H. Huang, S. Liu, T. B. Kornberg, Cytoneme-mediated contact-dependent transport of the Drosophila decapentaplegic signaling protein. *Science*. 343, 1244624 (2014).

20. L. González-Mendez, I. Seijo-Barandiarán, I. Guerrero, Cytoneme-mediated cell-cell contacts for Hedgehog reception. *Elife*. 6, 605 (2017).

21. W. Chen, H. Huang, R. Hatori, T. B. Kornberg, Essential basal cytonemes take up Hedgehog in the Drosophila wing imaginal disc. *Development*. 144, 3134–3144 (2017).

22. B. Mattes *et al.*, Wnt/PCP controls spreading of Wnt/β-catenin signals by cytonemes in vertebrates. *Elife*. 7, 180 (2018).

23. A. Sohr, L. Du, R. Wang, L. Lin, S. Roy, FGF cleavage is required for efficient intracellular sorting and intercellular dispersal. *J Cell Biol* (2019), doi:10.1083/jcb.201810138.

24. S. Saha, A. A. Anilkumar, S. Mayor, GPI-anchored protein organization and dynamics at the cell surface. *J. Lipid Res.* 57, 159–175 (2016).

25. I. W. Caras, An internally positioned signal can direct attachment of a glycophospholipid membrane anchor. *J Cell Biol*. 113, 77–85 (1991).

26. V. Greco, M. Hannus, S. Eaton, Argosomes: a potential vehicle for the spread of morphogens through epithelia. *Cell*. 106, 633–645 (2001).

27. G. I. Miura *et al.*, Palmitoylation of the EGFR ligand Spitz by Rasp increases Spitz activity by restricting its diffusion. *Developmental Cell*. 10, 167–176 (2006).

28. R. O. Hynes, Integrins: bidirectional, allosteric signaling machines. *Cell*. 110, 673–687 (2002).

29. H. Kohsaka, A. Nose, Target recognition at the tips of postsynaptic filopodia: accumulation and function of Capricious. *Development*. 136, 1127–1135 (2009).

30. J. B. A. Green, J. Sharpe, Positional information and reaction-diffusion: two big ideas in developmental biology combine. *Development*. 142, 1203–1211 (2015).

31. J. A. Porter, K. E. Young, P. A. Beachy, Cholesterol modification of hedgehog signaling proteins in animal development. *Science*. 274, 255–259 (1996).

32. K. Willert *et al.*, Wnt proteins are lipid-modified and can act as stem cell growth factors. *Nature*. 423, 448–452 (2003).

33. D. Yan, X. Lin, Shaping morphogen gradients by proteoglycans. *Cold Spring Harbor Perspectives in Biology*. 1, a002493–a002493 (2009).

34. R. Balasubramanian, X. Zhang, Mechanisms of FGF gradient formation during embryogenesis. *Semin. Cell Dev. Biol.* 53, 94–100 (2016).

35. K. Dejima, M. I. Kanai, T. Akiyama, D. C. Levings, H. Nakato, Novel contact-dependent bone morphogenetic protein (BMP) signaling mediated by heparan sulfate proteoglycans. *J. Biol. Chem.* 286, 17103–17111 (2011).

36. F. R. Taylor *et al.*, Enhanced potency of human Sonic hedgehog by hydrophobic modification. *Biochemistry*. 40, 4359–4371 (2001).

37. A. Gallet, L. Ruel, L. Staccini-Lavenant, P. P. Thérond, Cholesterol modification is necessary for controlled planar long-range activity of Hedgehog in Drosophila epithelia. *Development*. 133, 407–418 (2006).

38. A. Callejo, C. Torroja, L. Quijada, I. Guerrero, Hedgehog lipid modifications are required for Hedgehog stabilization in the extracellular matrix. *Development*. 133, 471–483 (2006).

39. K. F. Speer *et al.*, Non-acylated Wnts Can Promote Signaling. *CellReports*. 26, 875–883.e5 (2019).

40. C. Alexandre, A. Baena-Lopez, J.-P. Vincent, Patterning and growth control by membrane-tethered Wingless. *Nature*. 505, 180–185 (2014).

41. C. Cabernard, M. Affolter, Distinct roles for two receptor tyrosine kinases in epithelial branching morphogenesis in Drosophila. *Developmental Cell*. 9, 831–842 (2005).

42. N. M. Hooper, Determination of glycosyl-phosphatidylinositol membrane protein anchorage. *Proteomics*. 1, 748–755 (2001).

43. N. A. Dye *et al.*, Cell dynamics underlying oriented growth of the Drosophila wing imaginal disc. *Development*. 144, 4406–4421 (2017).

Acknowledgments

We thank Drs. N. Andrews and T.B. Kornberg for reading and comments on the manuscript; Drs. T.B. Kornberg and G. O. Barbosa for sharing the design of the culture chamber for live imaging; the Bloomington Stock Center for *Drosophila* lines; the Developmental Studies Hybridoma Bank for antibodies; Dr. A.E. Beaven for the help in the UMD imaging core facility. **Funding:** NIH grant R35GM124878 to SR. **Author Contributions:** A. Sohr discovered GPI-anchored Bnl and L. Du discovered its roles; S. Roy supervised the work and designed the project; L. Du and A. Sohr designed and conducted the experiments: S. Roy, L. Du, and A. Sohr wrote the paper. **Competing interests:** None declared.

Legends

Fig. 1. Bnl source and recipient cells extend cytonemes to contact each other. (A) Drawing depicting organization of the ASP, wing disc, myoblasts, and Btl-containing ASP cytonemes that directly receive Bnl from the disc *bnl* source. **(B)** Polarized ASP cytonemes (green; arrow) establish contacts with the wing disc *bnl* source (red). **(C)** Externalized Bnl^{ex} (red, αBnl^{ex}) is asymmetrically enriched on the source (dashed lined) and Btl:GFP-containing ASP cytoneme contact sites (arrow). **(D-D")** The wing disc *bnl* source (red) co-expressing Bnl:GFP and mCherryCAAX (*bnl-Gal4* X *UAS*-Bnl:GFP, *UAS-mCherryCAAX*); arrowhead, ASP-proximal area; arrow, Bnl:GFP containing cytonemes; dashed line, ASP; D", Bnl:GFP intensity profile within the boxed source area in the direction of the arrow in D' (see Fig. S1A-B). **(E,F)** 3D-rendered XZY views of the nlsGFP-marked ASP and mCherryCAAX-marked source cytonemes (arrow). **(G)** 3D-rendered views of two CD8:GFP-expressing clones within the *bnl* source area; arrow, cytonemes (see Fig. S1D,E; Table S1). **(H)** Violin plot showing the source cytoneme length distribution. **(I-K)** Dynamic contact-based interactions of source (red) and ASP (green) cytonemes; K, illustration of the results; arrowhead, contact sites. **(L,M)** Plots comparing ASP and source cytoneme dynamics (see Material and Methods; Fig. S1N,O; Table S2). All except C, live imaging. Scale bars, 20 μm; 5 μm (G).

Fig. 2. Bidirectional contact matchmaking of Bnl sending and receiving cytonemes. (A-E) Autonomous effects of Dia:GFP, DiaΔDAD:GFP and *diaRNAi* expression on cytonemes in mCherryAAX-marked source cells; all panels, 3D-rendered XZY views; E, graph showing source cytoneme numbers under indicated conditions; $p < 0.01$ for WT (n = 6) vs Dia (n = 6) or DiaΔDAD (n = 8) or *dia-i* (n = 6); (*UAS-mCherryCAAX;bnl-Gal4* X w^- for control, or *UAS-"*X"). **(F-H)** $Bnl:GFP^{endo}$ uptake in the ASP (dashed line) in control (*bnl:gfp*^{endo} X *bnl-Gal4*) and source cytoneme-depleted conditions (*UAS-dia-i, bnl:gfp*^{endo} X *bnl-Gal4*); H, violin plot showing levels of $Bnl:GFP^{endo}$ uptake in the ASP under indicated conditions; $p < 0.0001$, n = 7 (w^-) and 17 (*dia-i*); red, phalloidin-Alexa-647. **(I-K)** Non-autonomous effects of source cytoneme-

depletion on ASP cytonemes (CD2:GFP-marked); K, Plots comparing ASP cytoneme numbers under indicated conditions, $p < 0.0001$ for cytonemes >15 μm, n = 6 ASPs (control), 14 ASPs (*dia-i*); dashed arrow, ASP tip cytonemes. **(L-O)** Tracheal Btl:DN expression that removed ASP cytonemes also non-autonomously removed source cytonemes (red); O, graph showing correlation of source and ASP cytoneme numbers under partial Btl:DN conditions. **(P-P")** Bnl^{ex} (blue, αBnl^{ex}) localization at inter-cytoneme contacts in samples with partial Btl:DN phenotypes; P', split αBnl^{ex} channel; P", zoomed-in part of P. **(F-N)** dashed arrow, non-autonomous effects of the indicated genetic manipulation (arrow); arrowheads, inter-cytoneme contacts. All panels except F,G, P-P'', live imaging. Scale bars, 20 μm.

Fig. 3. Bnl is GPI anchored to the source cell surface. (A,A') Schematic map of the Bnl protein showing FGF domain, secreted signaling portion (left-right arrow), signal peptide (SP), signal sequence (SS), and sites for: furin cleavage (arrow), HA-tag (site #1), GFP-tag (site # 3), mCherry-tag, hydrophobicity plot (A'), and numbers, amino acid residues. **(B-E')** S2 cells co-transfected with *actin-Gal4* and *UAS-"X"* constructs and surface immuno-probed in non-permeabilized condition with either GFP or Bnl antibody, as indicated. **(B-B''')** In S2 cells, $Bnl:HA_1GFP_3Cherry_c$ (arrowheads) is cleaved intracellularly, and $Bnl:GFP_3^{ex}$ portion (arrow; blue) is surface localized; B'-B''', split channels. **(C-E)** Surface localization (red) of various constructs under pre-PIPLC and post-PIPLC conditions; CD8:GFP was co-expressed for untagged Bnl as an internal control; D, schematic maps of different Bnl constructs; E, E', Graphs comparing the ratio of surface (red) to total protein (GFP) expressed for indicated constructs and conditions (also see Fig. S2); ***, $p<0.001$, n=15 cells. **(F-K)** Surface Bnl^{ex} (red) levels on the wing disc *bnl* source (arrows) before and after PIPLC treatment; F-H, native Bnl in w^- control larvae; I-K, overexpressed Bnl under *bnl-Gal4*. **(L-R)** Source surface levels (red) of Bnl:GFP, Bnl:GFPΔC and Bnl:GFPΔC-TM on wing discs when expressed under *bnl-Gal4* (control) before and after PIPLC; R, graph comparing the fraction of source surface levels (red, αGFP^{ex}) to the total expression levels (green) of different variants;

n= 5 for each; only merged and red channels shown; arrows, source area; *, source-surrounding disc area; dashed line, ASP; Scale bars, 30 μm; 10 μm (B-C').

Fig. 4. GPI anchor ensures tissue-specific Bnl dispersion and interpretation. (A-C) Dispersion patterns of Bnl:GFP, Bnl:GFPΔC-TM (TM), or Bnl:GFPΔC (ΔC) from the wing discs *bnl* source (*UAS-mCherryCAAX; bnl-Gal4* X *UAS-"X"*); B, arrowhead, abnormal source membrane colocalized Bnl:GFPΔC-TM puncta; insets, zoomed-in ROI (box); dashed line, ASP; *, source-surrounding disc area; αDiscs large (Dlg), cell outlines. **(D-K)** Dispersion and signaling (dpERK, red) patterns of Bnl:GFP, TM, and ΔC when expressed from either the wing disc *bnl* source (D-F; *bnl-Gal4* x *UAS-"X"*) or ectopic GOF clones within the ASP (H-J; *hsFlp*; *btlenh>y+>Gal4, btlenh-mRFPmoe* x *UAS-"X"*); H-J insets, clone positions and signaling patterns (also see Fig. S3H-K); D-J; arrow and arrowhead, signal-recipient cells with and without nuclear dpERK, respectively; G, average intensity plots comparing Bnl:GFP, TM, and ΔC distribution along the ASP D-P axis; K, violin plots comparing the percentage of signal-receiving ASP cells with nuclear dpERK from overexpression (OE) and clonal expression; $p < 0.01$: ΔC (n = 16) vs either Bnl:GFP (n = 17) or TM (n = 13) under OE; see Fig. S3K for p values for clonal assays. **(L-O)** Levels of tracheal branch invasion (arrows) on larval salivary glands expressing either Bnl:GFP, TM, or ΔC (*bnl-Gal4* X *UAS-X*); L-N, brightfield, 10X magnification; O, Sholl analyses graph comparing frequency of terminal branching. **(P-S)** Fraction of Bnl:GFP, TM, and ΔC displayed on the basal surface (red, αGFP^{ex}) when expressed from salivary glands; S, graph comparing the fraction of surface displayed signals (arrowhead); arrow, cell junctions; $p < 0.05$: Bnl:GFP (n = 17) vs TM (n = 26), $p < 0.01$: ΔC (29) vs either Bnl:GFP or TM. Scale bars, 30 μm; 100 μm (L-N); 20 μm (P-R').

Fig. 5. GPI-anchored Bnl acts as a CAM to drive bidirectional cytoneme contact matchmaking. (A-I) Effect on the reciprocal polarity and numbers of ASP and source cytonemes (arrows) when either Bnl:GFP, Bnl:GFPΔC, or Bnl:GFPΔC-TM were expressed from the disc source (also see Fig.S4A-G); A,D,G, extended Z- projection,

both the ASP (red) and source (blue) are genetically marked; A, inset, ROI (box) in green and blue channels; B,E,H, 3D-rendered views, only source membrane marked (red); dashed lines, ASP; B', only red channel of B; D,E, dashed arrows, randomly oriented short cytonemes devoid of signal localization; C,F,I, R-plots comparing numbers, length, and polarity of ASP and source cytonemes (also see Fig. S4H,I). **(J-J')** 3D projection of cytonemes from the ASP (*btl>CherryCAAX*) and the Bnl:GFPΔC-TM - expressing wing disc *bnl* source (blue, *bnl>CD4:IFP2*); J', orthogonal views showing a Bnl:GFPΔC-TM puncta (arrow) at an inter-cytoneme junction. All panels, live imaging; dashed line, ASP outline. Scale bars, 20 μm.

Fig. 6. Btl-Bnl-interactions mediate cytoneme contact assembly and plasticity. (A-B) 3D-projected images of cytonemes from the Bnl:GFPΔC-TM-expressing wing disc *bnl* source (blue, *bnl>CD4:IFP2*) in *btl:cherry*^{endo} knock-in larvae; Co-clustering of Btl:Cherry^{endo} puncta (red) from the ASP and Bnl:GFPΔC-TM puncta (arrows) from the source at the inter-cytoneme contact sites. **(C,D)** Violin plots showing the maximum extension and lifetime (C) and average extension and retraction velocity (D) of ASP (recipient) and source cytonemes while source cells expressed Bnl:GFPΔC-TM (also see Table S2 for comparison and statistical significance). All panels, live imaging. **(E)** Proposed model showing how GPI-anchored Bnl ensures tissue-specific cytoneme contact matchmaking, contact-dependent exchange, and bidirectional signaling feedback to self-sustain signaling sites. Scale bars, 20 μm.

Figure 1

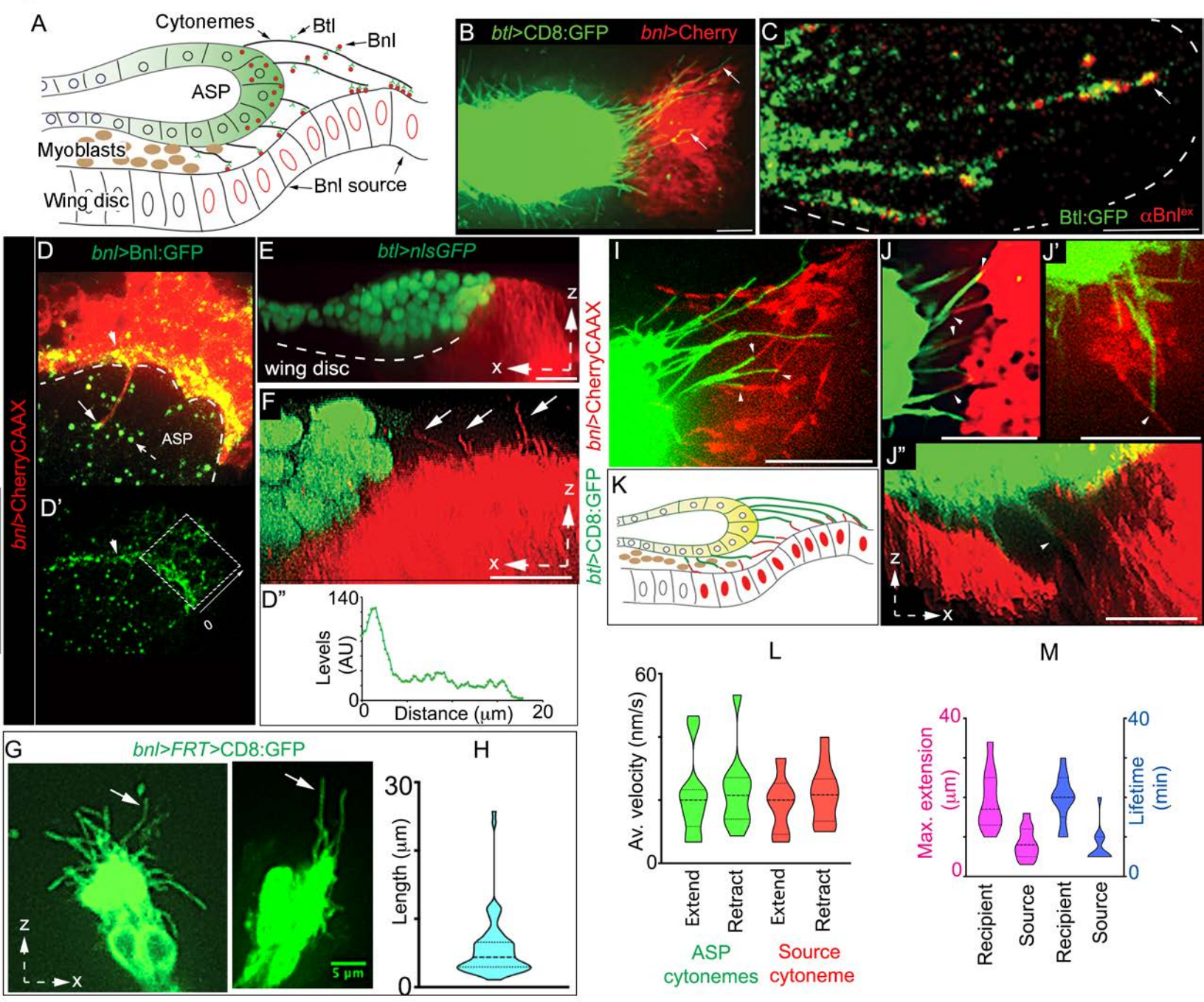

Figure 2

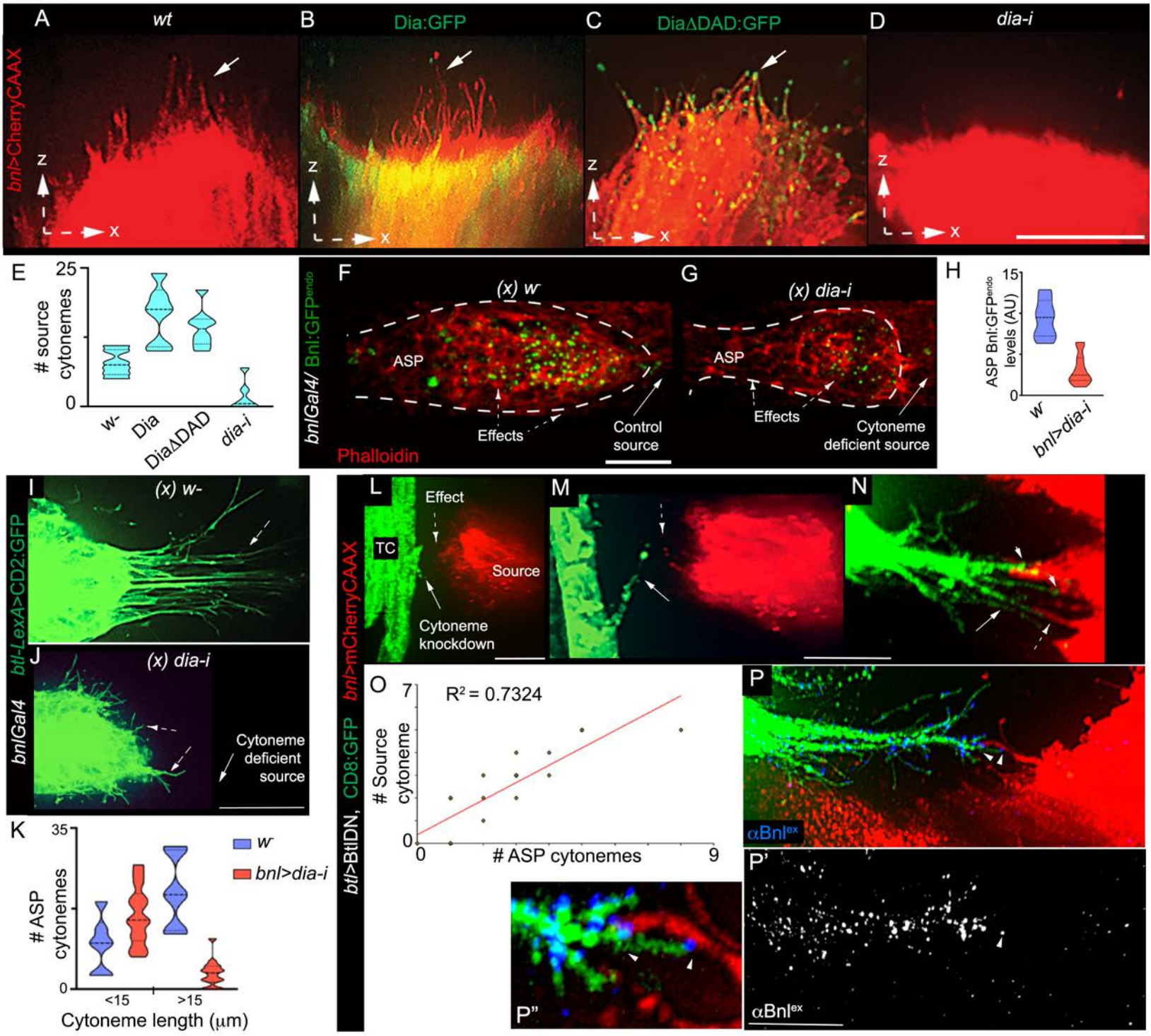

Figure 3

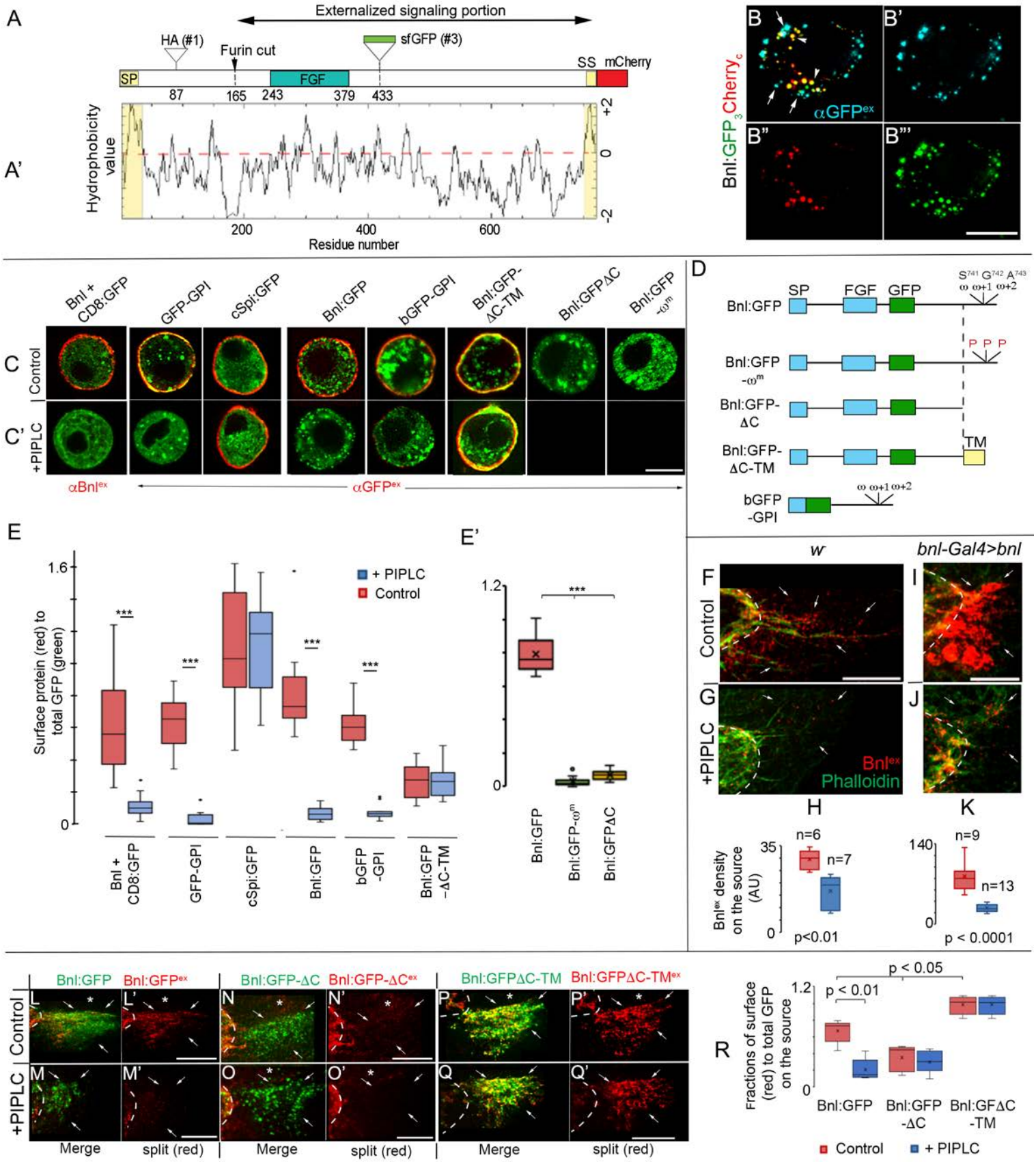

Figure 4

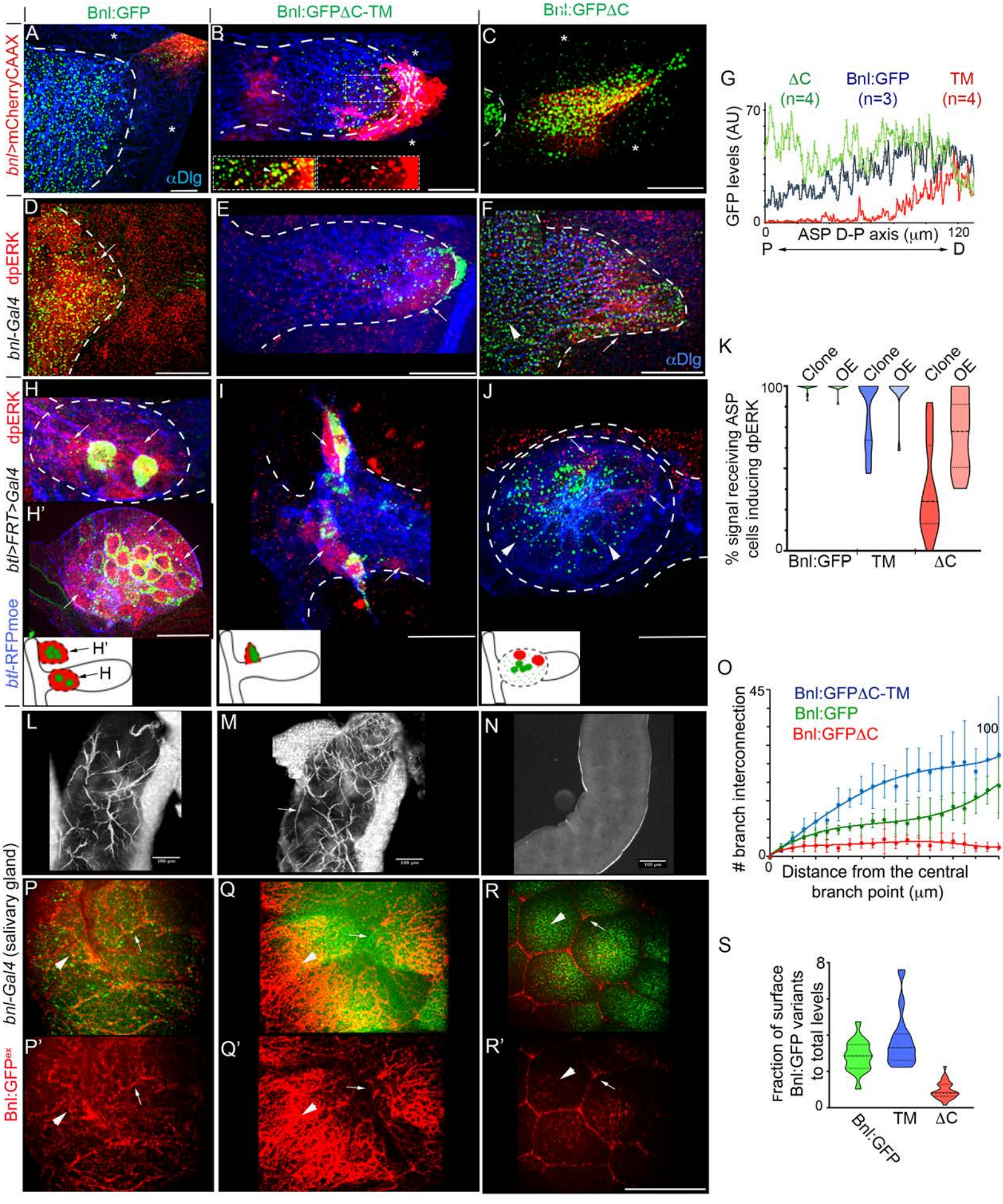

Figure 5

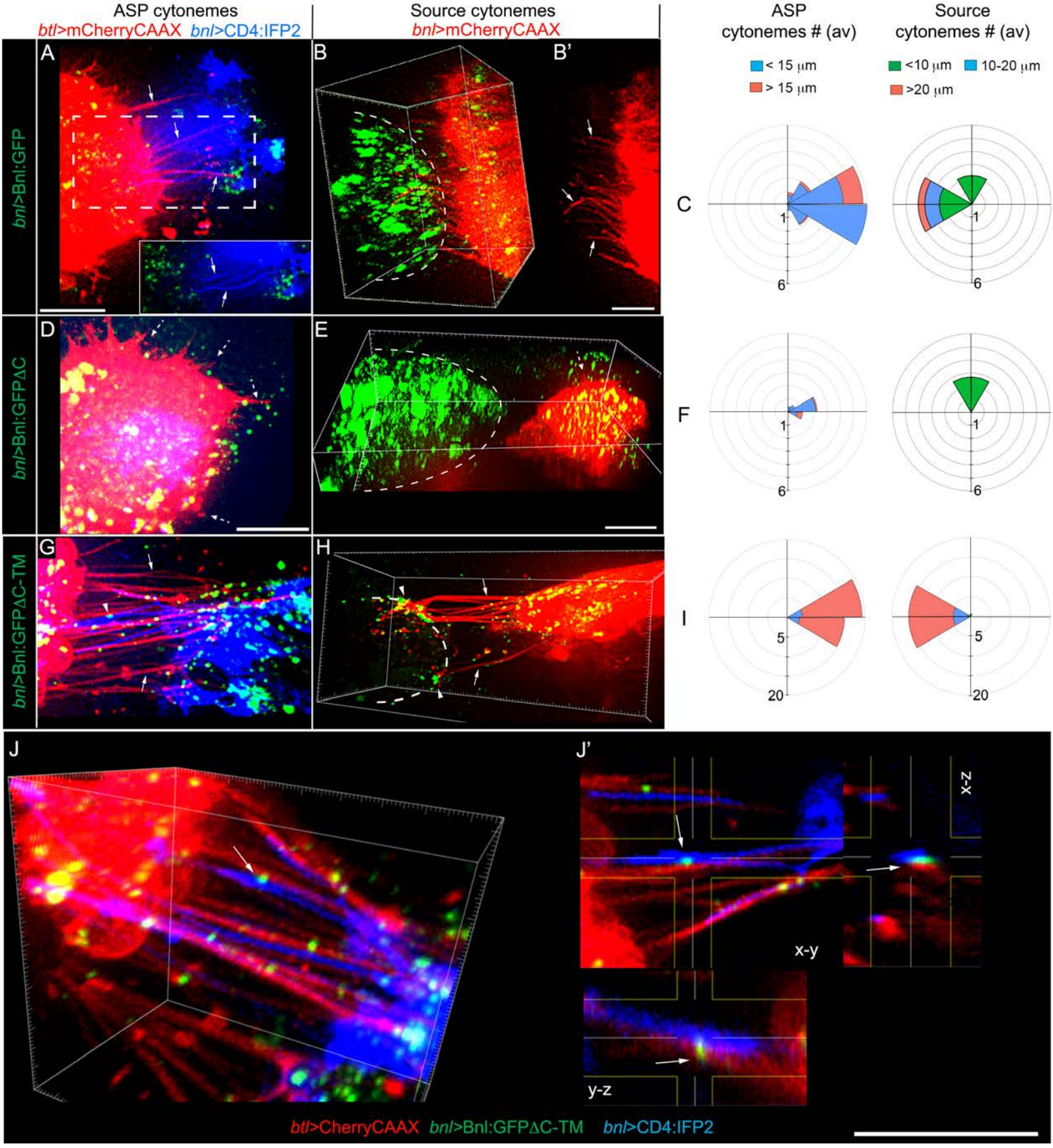

Figure 6